Structural Basis for Novel δ-Regioselective Heme Oxygenation in the Opportunistic Pathogen *Pseudomonas aeruginosa*[†,‡]

Jonathan Friedman,[§] Latesh Lad,[§] Huiying Li,[§] Angela Wilks,[||] and Thomas L. Poulos*[,§]

Department of Molecular Biology and Biochemistry, Department of Physiology and Biophysics, and Program in Macromolecular Structure, University of California, Irvine, California 92697, and Department of Pharmaceutical Sciences, School of Pharmacy, University of Maryland, Baltimore, Maryland 21201

Received February 11, 2004; Revised Manuscript Received March 8, 2004

ABSTRACT: The Gram-negative bacterium *Pseudomonas aeruginosa* contains a heme oxygenase (*pa*-HO) that primarily oxygenates the δ-*meso* heme carbon [Caignan, G. A., Deshmukh, R., Wilks, A., Zeng, Y., Huang, H. W., Moenne-Loccoz, P., Bunce, R. A., Eastman, M. A., and Rivera, M. (2002) *J. Am. Chem. Soc. 124*, 14879−14892]. This differs from other previously characterized heme oxygenases, which display regioselectivity for the α-*meso* heme carbon. Here we report the crystal structure of *pa*-HO at 1.60 Å resolution and compare it to the 1.50 Å structure of *nm*-HO from *Neisseria meningitidis* [Schuller, D. J., Zhu, W., Stojiljkovic, I., Wilks, A., and Poulos, T. L. (2001) *Biochemistry 40*, 11552−11558]. The crystal structure of *pa*-HO maintains the same overall fold as other bacterial and mammalian heme oxygenases, including a conserved network of hydrogen-bonded solvent molecules important for dioxygen activation. The novel δ-regioselectivity of heme oxygenation observed by *pa*-HO is due to the heme being rotated by ∼100°, which places the δ-*meso* heme carbon in the same position as the α-*meso* heme carbon in other heme oxygenases. The main interaction in *pa*-HO that stabilizes the unique heme orientation is a salt bridge between Lys132 and the heme 7-propionate, as well as hydrophobic contacts involving Leu29, Val33, and Phe189 with the heme methyl and vinyl groups.

Heme oxygenase (HO)[1] catalyzes the initial steps in heme degradation. The overall heme oxygenase reaction involves a sequence of transformations that consumes three molecules of O_2 and seven electrons (Figure 1). The first electron reduces the ferric heme iron to the ferrous state, followed by O_2 binding to form a dioxygen complex. Addition of a second electron and one proton to the oxy complex generates a reactive hydroperoxy intermediate, Fe(III)-OOH (*1*). In most heme oxygenases the Fe(III)-OOH hydroxylates the α-*meso* heme position to give ferric α-*meso*-hydroxyheme (*1*, *2*). This differs from cytochromes P450 and peroxidase enzymes, which heterolytically cleave the O−O bond to generate a ferryl Fe(IV)-O species (*3*). The crystal structures of human and rat HO-1 (*4*, *5*), and bacterial *nm*-HO and *cd*-HO (*6*, *7*) suggest that the α-regioselectivity of the reaction is likely to be controlled by steric interactions between the distal helix and the heme. Furthermore, hydrogen-bonding interactions within the active site may help to orient molecular oxygen toward the α-*meso* carbon. Upon reaction with one molecule of O_2 and one electron, α-*meso*-hydroxyheme is converted to verdoheme, with release of the α-*meso* carbon as CO (*8*−*10*). The conversion of verdoheme to the biliverdin product is not well understood but does require both molecular oxygen and reducing equivalents (*11*, *12*).

HO has been identified in a large number of organisms, including higher green plants, red algae, and cyanobacteria, where the HO reaction is required for the formation of open-chain tetrapyrrole pigments, phytobilins (*13*). In mammals the product CO has been implicated as a neuronal second-messenger molecule in various physiological pathways (*14*−*18*), while biliverdin and its reduced form, bilirubin, may work as physiological antioxidants (*19*−*21*). Of particular interest, HO is present in some pathogenic bacteria including *Corynebacterium diphtheriae*, *Neisseria meningitidis*, and *Neisseria gonorrheae*. In the Gram-negative pathogens *N. meningitidis* and *N. gonorrheae*, HO was shown to be necessary for bacterial utilization of iron from imported heme (*22*).

Recently, a heme oxygenase from *Pseudomonas aeruginosa* (*pa*-HO) was identified by its high amino acid sequence identity (37%) with a heme oxygenase from *N. meningitidis* (*nm*-HO) (*23*). *P. aeruginosa* is an opportunistic pathogen that causes a variety of systemic infections, particularly in those afflicted with cystic fibrosis, as well as cancer and AIDS patients who are immunosuppressed (*24*, *25*). *P. aeruginosa* prefers anaerobic metabolism, which requires micromolar quantities of host iron for optimal growth (*26*). Because there is essentially no free iron in mammals (*27*), *pa*-HO is critical for the acquisition of host iron. *pa*-HO is unusual since it hydroxylates heme predominantly at the

[†] This work was supported by NIH Grants GM33688 (to T.L.P.) and AI55912 (to A.W.).

[‡] PDB coordinates and structural factors have been deposited in the Protein Data Bank under Accession Number 1SK7.

* To whom correspondence should be addressed: tel (949) 824-7020; fax (949) 824-3280; e-mail poulos@uci.edu.

[§] University of California.

[||] University of Maryland.

[1] Abbreviations: HO, heme oxygenase; *nm*-HO, *N. meningitidis* HO; *pa*-HO, *P. aeruginosa* HO; heme, Fe-protoporphyrin IX; RMS, root-mean-square.

10.1021/bi049687g CCC: $27.50
Published on Web 04/17/2004

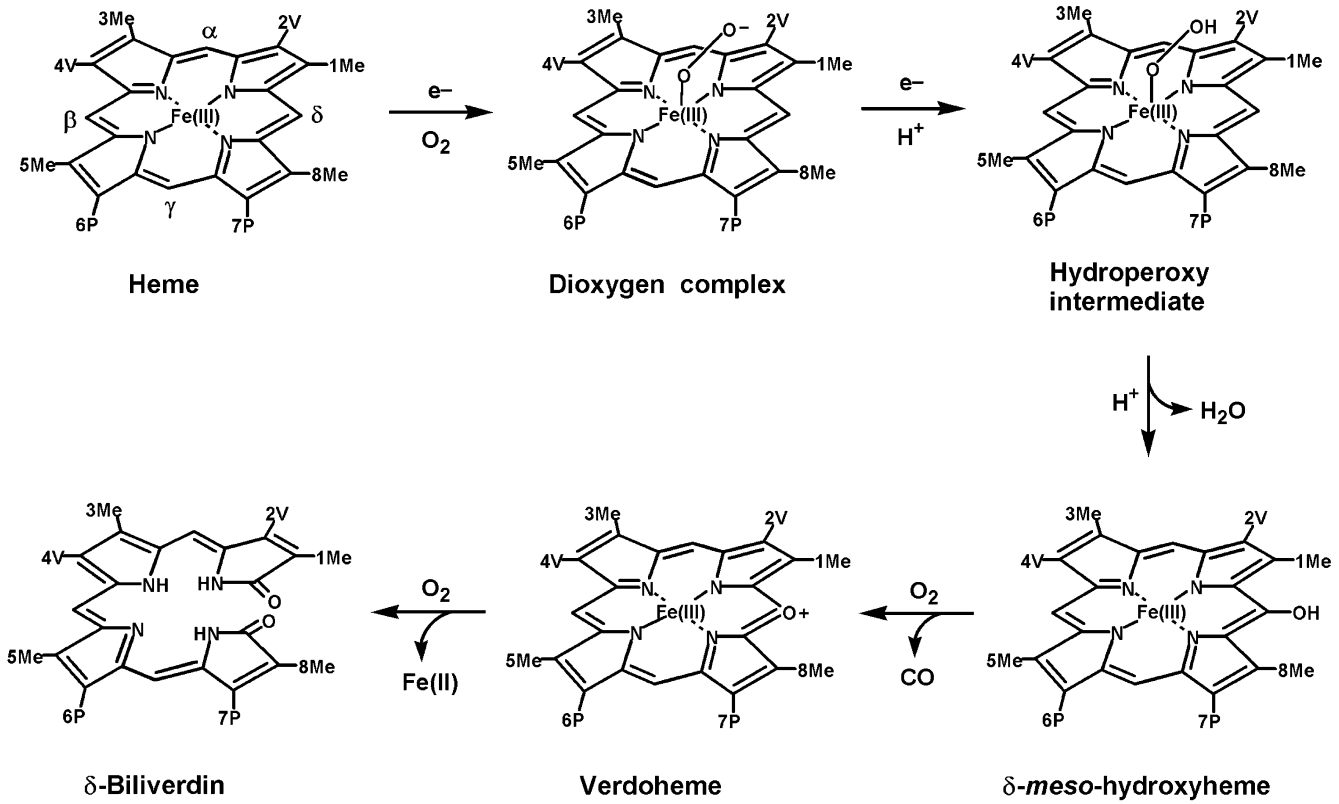

FIGURE 1: Overall reaction catalyzed by *P. aeruginosa* heme oxygenase (*pa*-HO) as defined by the studies of mammalian heme oxygenases and *cd*-HO from *C. diphtheriae*. Substituents are numbered 1−8, and abbreviations are given by Me (methyl group), V (vinyl group), and P (propionic acid group). All heme oxygenases characterized thus far oxidize the porphyrin ring at the α-*meso* carbon, whereas *pa*-HO oxidizes heme primarily at the *δ-meso* carbon.

δ-meso carbon (*28*), while all other well-studied HOs hydroxylate the α-*meso* carbon (*29*−*31*). However, mutants of HO-1 have been shown to exhibit altered regioselectivity. For example, mutating Arg183 in rat HO-1 leads to the formation of *δ*-biliverdin, suggesting that heme propionate−protein interactions are important in controlling regioselectivity (*32*). Here we report the crystal structure of *pa*-HO at 1.60 Å resolution and compare it to the 1.60 Å structure of *nm*-HO (*6*), which provides important insights into factors that control the unique regioselectivity of heme oxygenation by *pa*-HO.

EXPERIMENTAL PROCEDURES

Expression of pa-HO. The *Escherichia coli* BL21(DE3) strain carrying pWMZ1656 (*pigA*) was expressed as previously described (*23*). A single colony of freshly transformed cells was cultured overnight at 37 °C in 5 mL of LB medium containing 100 μg/mL ampicillin. The cells were subsequently subcultured into fresh LB-ampicillin medium (100 mL) and grown at 37 °C to mid-log phase. These cells were then subcultured (10 mL) into fresh LB-ampicillin medium (1 L), and upon reaching mid-log phase, expression was induced by addition of isopropyl 1-thiogalactopyranoside (IPTG) to a final concentration of 1 mM. The cells were grown further for ∼4 h at 28−30 °C and harvested by centrifugation (5500 rpm for 15 min). The resulting cell pellet was green due to the conversion of endogenous *E. coli* heme to biliverdin by the expressed *pa*-HO protein.

Purification of pa-HO and Reconstitution with Heme. Purification of the recombinant *pa*-HO protein and its reconstitution with heme were carried out as previously described (*23*). The cell pellet was resuspended in 20 mM Tris-HCl (pH 7.8) containing 1 mM EDTA and 1 mM phenylmethanesulfonyl fluoride (PMSF), and the mixture was allowed to stir at 4 °C for 1 h. The cells next were lysed by sonication and centrifuged at 18 000 rpm for 1 h. The soluble fraction was applied to a Sepharose-Q Fast Flow column (1.5 × 10 cm) previously equilibrated with 20 mM Tris-HCl (pH 7.6). The column was washed with three volumes of 20 mM Tris-HCl (pH 7.6), and the protein was eluted in the same buffer by a linear gradient of NaCl from 0 to 500 mM. Peak fractions were pooled together on the basis of SDS−PAGE analysis, and the purified protein was dialyzed against 20 mM Tris-HCl (pH 7.6, 2 × 4 L) at 4 °C. Hemin was then added to the *pa*-HO sample at a final 2:1 heme:protein molar ratio, and the heme−*pa*-HO complex was applied to a Sepharose-Q Fast Flow column (1.5 × 6.0 cm) previously equilibrated with 20 mM Tris-HCl (pH 7.6). The column was washed with three volumes of 20 mM Tris-HCl (pH 7.6), and the protein was eluted in the same buffer by a linear gradient of NaCl from 0 to 500 mM. Peak fractions were pooled together and dialyzed against 20 mM Tris-HCl (pH 7.6) (2 × 4 L), and the sample was then applied to a Sephacryl S-100 HR column (3.0 × 100 cm) previously equilibrated in the same buffer. The final purified *pa*-HO protein was concentrated by Amicon filtration unit and stored at −80 °C.

Crystal Growth and Data Collection. Optimized conditions for crystallization of *pa*-HO consisted of vapor diffusion with the reservoir containing 2.3 M ammonium sulfate, 0.1 M Tris-HCl, pH 8.5, 2.0% Jeffamine ED-600 (Fluka), and sitting drops consisted of 5 μL of reservoir buffer and 5 μL

of protein stock at 18 mg/mL. Crystals grew after 2 weeks at room temperature. The crystals belong to monoclinic space group *C*2 with cell dimensions $a = 86.03$ Å, $b = 51.80$ Å, $c = 63.92$ Å, and $\beta = 131.0°$ with one molecule per asymmetric unit. Preparation of crystals suitable for cryogenic data collection required the use of D-(+)-trehalose as a cryoprotectant. Crystals were soaked by a three-step process into reservoir buffer containing increasing amounts of D-(+)-trehalose to a final concentration of 30% (w/v) and flash-frozen by cold nitrogen stream. A 2.5 Å data set with high redundancy (250° scan) was collected in-house on an R-axis IV imaging plate equipped with a Rigaku RU-H3R X-ray generator and Osmic focusing optics. High-resolution diffraction data sets of *pa*-HO were collected on single crystals by use of synchrotron radiation of 1.0 Å wavelength at the Advanced Light Source (Berkeley, CA), beamline 5.0.1. Data sets consisted of 130 frames with a ϕ rotation of 1°/frame. Data were integrated and scaled by use of HKL-2000 and SCALEPACK (*33*), with rejections performed with ENDH-KL (Louis Sanchez, California Institute of Technology) in conjunction with SCALEPACK.

Structure Solution and Refinement. The *pa*-HO structure was determined by the molecular replacement method by use of AMORE from the CCP4 suite (*34*). A search model was constructed from the protein moiety of *nm*-HO (PDB code 1J77) by mutating all residues to Ala. Rotation and translation function searches identified one solution with a correlation coefficient of 0.54 and *R* factor of 50.4% at 5.0 Å resolution. Packing analysis of all symmetry mates in the unit cell revealed some clashing between a surface loop of the *nm*-HO model and a neighboring molecule. Thus, the molecular replacement calculation was repeated after removal of the loop region (residues 90−100) from the search model. The final solution from AMORE was confirmed by observation of a 10σ peak at the expected heme iron position, which was generated by an anomalous difference Fourier synthesis using model phases. To further improve the quality of the electron density maps, heme iron coordinates were provided to SHARP (*35*) for refinement of the single anomalous dispersion (SAD) phases from the 2.5 Å in-house data set. The SAD phases were then combined with the molecular replacement model phases and further modified by use of DM from the CCP4 suite, including solvent flattening and histogram matching. The electron density maps calculated from the combined phases were better quality than the maps calculated from the molecular replacement model phases alone. The protein side chains of a *pa*-HO model, as well as the truncated loop region, were built into the electron density maps with the program O (*36*). Early rounds of refinement with CNS (*37*) included rigid-body minimization, simulated annealing, and *B*-factor refinement. Electron density maps generated from a 1.60 Å data set were used for further refinement of the *pa*-HO structure to a final *R* factor of 0.235 and R_{free} factor of 0.273. Backbone geometry was checked in PROCHECK (*38*), and none of the residues were in the disallowed region. During refinement, water molecules were manually added to the *pa*-HO structure in CNS and checked through visual inspection of their positions in both $2F_o - F_c$ and $F_o - F_c$ maps. In addition, one sulfate anion was assigned to the electron density. Data collection and refinement statistics are summarized in Table 1.

Table 1: Data Collection and Refinement Statistics

radiation source	synchrotron
wavelength (Å)	1.00
oscillation angle (deg)	1.0
measurement angle (deg)	130
Crystallographic Data	
space group	*C*2
a (Å)	86.03
b (Å)	51.80
c (Å)	63.92
molecules per unit cell	1
resolution (Å)	1.60
mosaicity (deg)	0.91
total observations	101 421
unique reflections	30 788
completeness[a] (%)	99.6 (95.9)
R_{merge}[b] (%)	5.3 (41.0)
mean I/σ	27.4 (2.27)
Refinement Statistics	
R_{cryst}[c]	0.235
R_{free}	0.273
rmsd bond lengths (Å)	0.010
rmsd angles (deg)	1.322
no. of water molecules	158
Ramachandran Angles	
most favored (%)	94.5
additional allowed (%)	5.5
generously allowed (%)	0.0

[a] Completeness is given for all data and highest resolution shell. [b] $R_{merge} = \sum I - \langle I \rangle / \sum I$. [c] $R_{cryst} = \sum |F_{obs}| - k|F_{calc}| / \sum |F_{obs}|$. R_{free} is the R_{cryst} calculated on the 5% of reflections excluded from refinement.

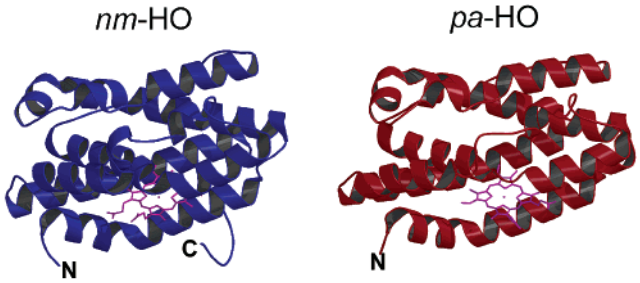

FIGURE 2: Ribbon representations of the overall structures of *nm*-HO and *pa*-HO. The heme substrate in both enzymes is shown in magenta. The N and C termini are labeled with the exception of the *pa*-HO C-terminus, which is hidden in this view. This figure was prepared with MOLSCRIPT (*46*).

RESULTS AND DISCUSSION

Overall Structure. The 1.60 Å crystal structure of *pa*-HO in a complex with heme has been solved by the molecular replacement method, with *nm*-HO as a search model. The first 11 residues of *pa*-HO are not ordered in the electron density map, and thus the *pa*-HO structure begins with Asn12 at the N-terminus and ends with Ala198 at the C-terminus. In *nm*-HO, the C-terminus wraps around toward the front of the active site, whereas the corresponding C-terminal region in *pa*-HO is not present due to a shorter amino acid sequence. Superimposition of the folds of *nm*-HO and *pa*-HO reveals that the two enzymes, as expected, share a homologous and largely α-helical fold (Figure 2), with an overall RMS deviation of 0.85 Å. In contrast, the overall RMS deviation between *nm*-HO and human HO-1 is 1.73 Å (*6*), indicating a higher degree of structural similarity between the two bacterial enzymes.

Heme Coordination Environment. The heme iron is six-coordinate with the imidazole group of His26 providing the

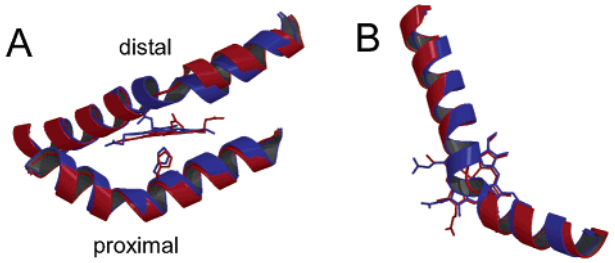

FIGURE 3: **(**A**)** Superimposition of the proximal and distal helices in *nm*-HO (blue) and *pa*-HO (red) **(**B**)** The distal helices both have ~50° kink directly above the heme surface, which is introduced by the glycines of the highly conserved sequence Gly-Ser-X-Leu-Gly. This kink is thought to provide the flexibility required for binding of the heme substrate and release of the biliverdin product.

proximal heme ligand. The orientation of the His ligand ring also is the same in both structures, such that the plane of the imidazole ring roughly bisects the vectors defined by the pyrrole N−Fe−N bonds. In both *nm*-HO and *pa*-HO, a neighboring carboxylate can accept a hydrogen bond from the proximal His ligand. In *nm*-HO, Asp24 directly H-bonds with His23, but in *pa*-HO, Glu30 interacts with His26 through a bridging water molecule that is located 2.75 Å from the Nδ atom of His26 and 2.89 Å from the Oϵ atom of Glu30. A similar bridging interaction was also identified in the crystal structure of *cd*-HO (*7*), involving Glu24, a nearby water molecule, and the proximal His20 ligand. A water molecule serves as the other axial ligand, consistent with previously reported spectroscopic and mutagenesis results (*23*, *28*). The carbonyl oxygen of both Gly121 and Leu124 are within H-bonding distance of the distal water ligand, 3.21 and 2.87 Å, respectively.

Distal Helix and Heme Pocket. Superimposition of the proximal and distal helices of *nm*-HO and *pa*-HO is shown in Figure 3A. An important structural feature identified in all heme oxygenases studied thus far is the distortion in the distal helix that covers part of the heme surface (Figure 3B). Such distortions and flexibility are generally considered important for the catalytic mechanism (*39*, *40*). With human HO-1, distinct differences are observed in the position of the distal helix relative to the heme in the two molecules of the asymmetric unit (*4*). One molecule has the distal helix further from the heme and has been termed the "open" conformation, while the other adopts a more "closed" conformation with the distal helix positioned closer to the heme. In addition, differences have been noted between the distal helix in human HO-1 and the highly homologous rat HO-1 (*41*, *42*). $2F_o - F_c$ composite-omit electron density maps indicate that the heme and distal helix in *pa*-HO are well-ordered (Figure 4). By comparison with other known HO structures, the distal helix in the *pa*-HO structure adopts the closed conformation. Furthermore, the side-chain OH group of Ser117 in *nm*-HO and Ser122 in *pa*-HO forms hydrogen bonds with the peptide backbone, which helps to stabilize the distal helix distortion. Throughout the distal helix region only one residue is not structurally conserved between *nm*-HO and *pa*-HO. As shown in Figure 5, Asn118 in *nm*-HO points up and away from the heme but is replaced by Lys123 in *pa*-HO. In *nm*-HO there is a concerted motion of Asn118 and Arg77 in going from the Fe(II) to the Fe(II)-NO structure. Asn118 swings up while Arg77 swings down to complete an H-bonded network with the iron-linked NO that is very likely important for catalysis (*43*). In *pa*-HO, Arg80 points down toward the heme as in the *nm*-HO Fe(II)-NO structure, and hence, Arg80 in *pa*-HO is already in the "activated" position. This difference is most likely due the replacement of Asn118 in *nm*-HO with Lys123 in *pa*-HO, which precludes, owing to potential steric clashes, the concerted motion observed in *nm*-HO.

All known HO structures, including *pa*-HO, contain a network of hydrogen bonds within the distal heme pocket between key side chains and ordered solvent molecules. This rigid network of H-bonded water molecules ensures proper proton delivery to the distal O atom of the iron-bound O_2 ligand and helps to stabilize the active HO hydroxylating

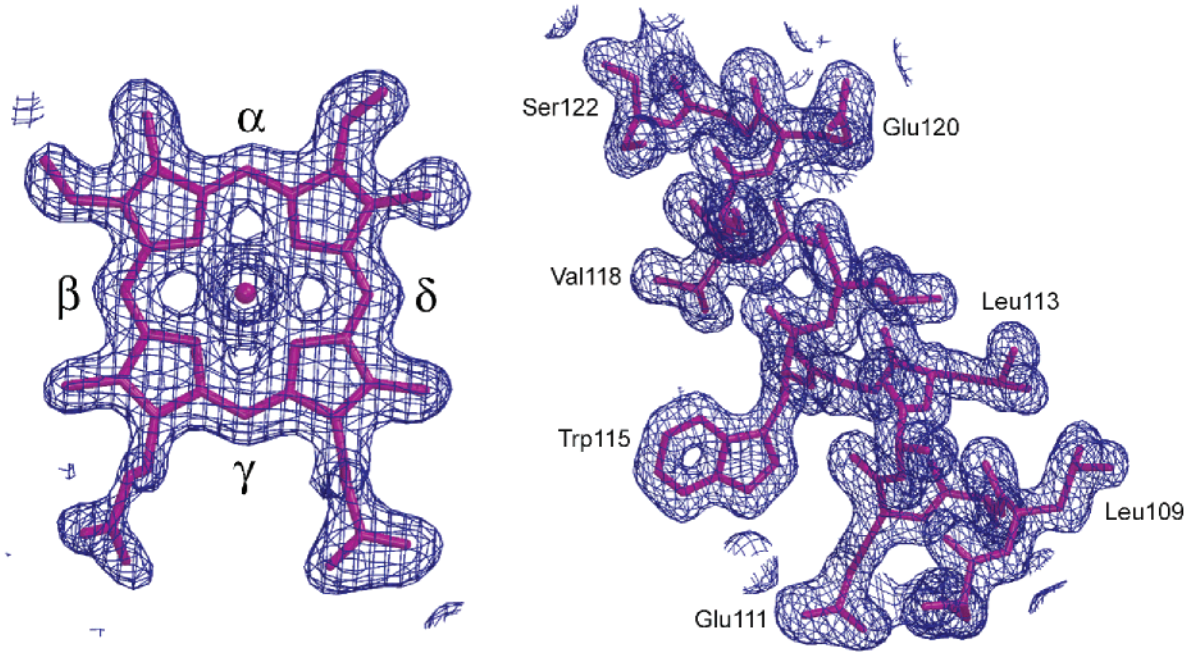

FIGURE 4: $2F_o - F_c$ composite-omit electron density maps contoured at 1σ showing the heme prosthetic group (left) and part of the distal helix (right). This figure was prepared with BOBSCRIPT (*47*).

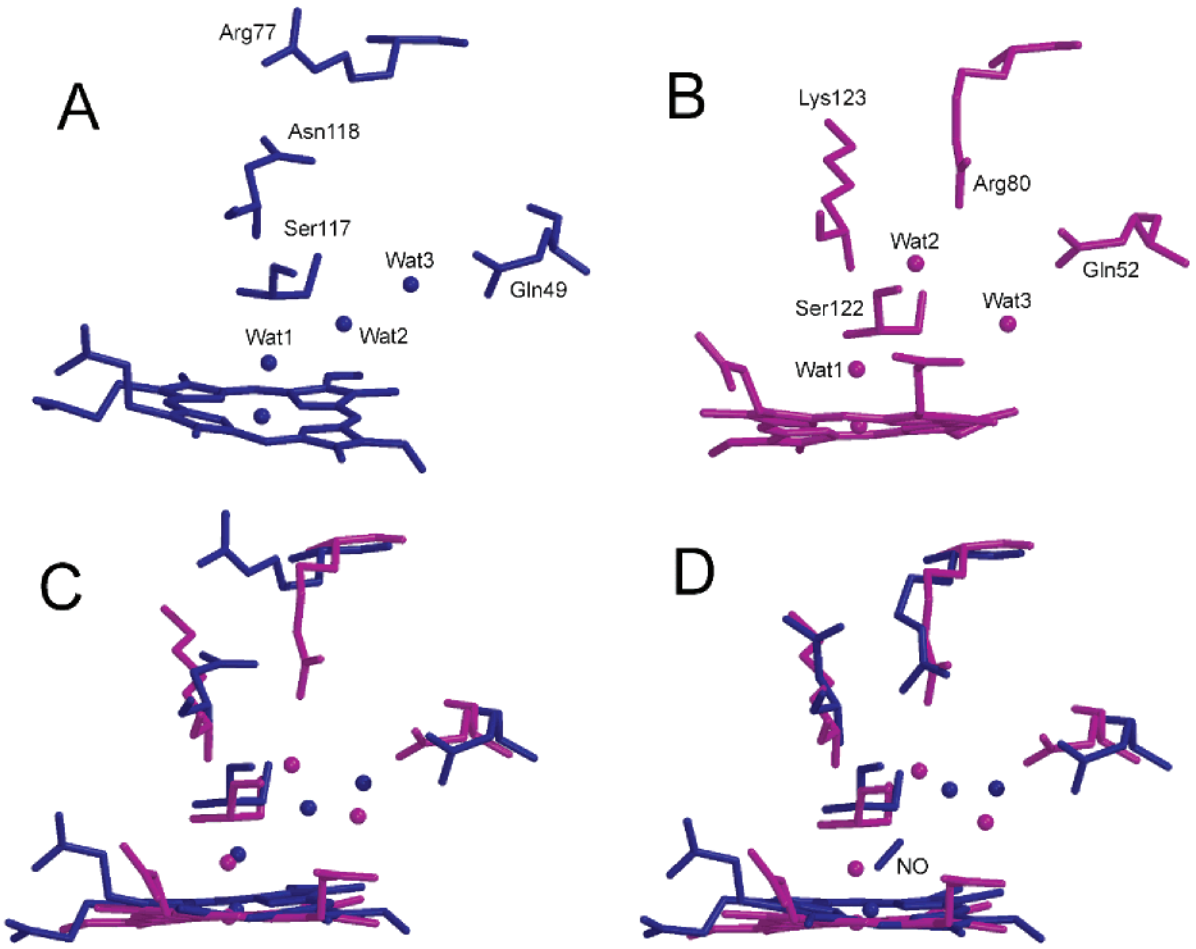

FIGURE 5: **(A)** Active-site structure of *nm*-HO. **(B)** Active-site structure of *pa*-HO. **(C)** Superimposition of the active-site structures of *nm*-HO (blue) and *pa*-HO (magenta). **(D)** Superimposition of the "activated" conformation of the NO-bound *nm*-HO complex (blue) and *pa*-HO (magenta).

species, Fe(III)-OOH. In human HO-1, Thr135 and Asp140 directly participate in this H-bonded network, whereas residues of different size and charge are utilized in *nm*-HO and *pa*-HO (Figure 5). Although the active-site residues differ between bacterial and mammalian heme oxygenases, the close similarity in the H-bonded water networks suggests a common catalytic mechanism shared by all HO enzymes.

Heme Orientation and Propionate Interactions. NMR studies of human HO-1 indicate that the heme has two orientations rotated by 180° along the α−γ *meso* axis (*44*). This is consistent with the observed hydroxylation of heme by *pa*-HO such that both the *β*- and *δ*-*meso* heme carbons are oxidized with *δ*-*meso* hydroxylation favored (*28*). The $2F_o - F_c$ electron density for the heme methyl, vinyl, and propionate groups are well-defined, indicating a single heme orientation in the *pa*-HO crystal structure.

The reason *pa*-HO gives a 70:30 mixture of *δ*-hydroxy- and *β*-hydroxyhemes, respectively, is readily understood from the *pa*-HO crystal structure. The heme in *pa*-HO is rotated by ∼100° such that the *δ*-heme edge is positioned toward the back end of the active-site pocket rather than the α-heme edge as in other HOs. Using NMR methods, Caignan et al. (*28*) also concluded that the heme in *pa*-HO is rotated ≈110° relative to the α-*meso* hydroxylating HOs. This structural difference is a result of different interactions between the protein and heme propionates. In *nm*-HO, these interactions involve Lys16 and Tyr112 (Lys18 and Tyr134 in human and rat HO-1), but the corresponding residues in *pa*-HO are Asn19 and Phe117, respectively (Figure 6). Table 2 provides a list of heme−protein contacts in various HOs. Furthermore, there are no basic side chains in *pa*-HO that correspond to Lys179 and Arg183 in mammalian HO-1, which are important for proper heme positioning through charge interactions with the heme propionates (*4*, *41*). Zhou et al. (*32*) showed that mutation of Arg183 in rat HO-1 leads to the formation of *δ*-biliverdin. One possible explanation presented by Zhou et al. is that the heme rotates in the active site (*32*). Interestingly, Trp158 in *pa*-HO occupies the space taken by Arg183 in mammalian HO-1 and may partly explain the unique *δ*-regioselectivity observed by *pa*-HO. As shown in Figure 6, Lys132 provides the key interaction with a heme propionate in *pa*-HO that stabilizes the heme in a unique orientation. On the basis of mutagenesis experiments, Fujii et al. (*45*) concluded that Lys34 in *pa*-HO may also hydrogen-bond with a heme propionate. The crystal structure of *pa*-HO indicates that Lys34 does not form a direct hydrogen bond with a heme propionate but may be close enough (6.3 Å) to provide a weak electrostatic interaction. The distance between the Nϵ atom of Lys132 and the heme 7-propionate is 2.8 Å and is thus the dominant interaction in *pa*-HO that controls *δ*-regioselectivity. Furthermore, the heme 1-methyl group is located 3.3 Å from Leu29, and the heme 8-methyl group is located within contact distance (4.2 Å) from the C*β* atom of Val33. These two hydrophobic

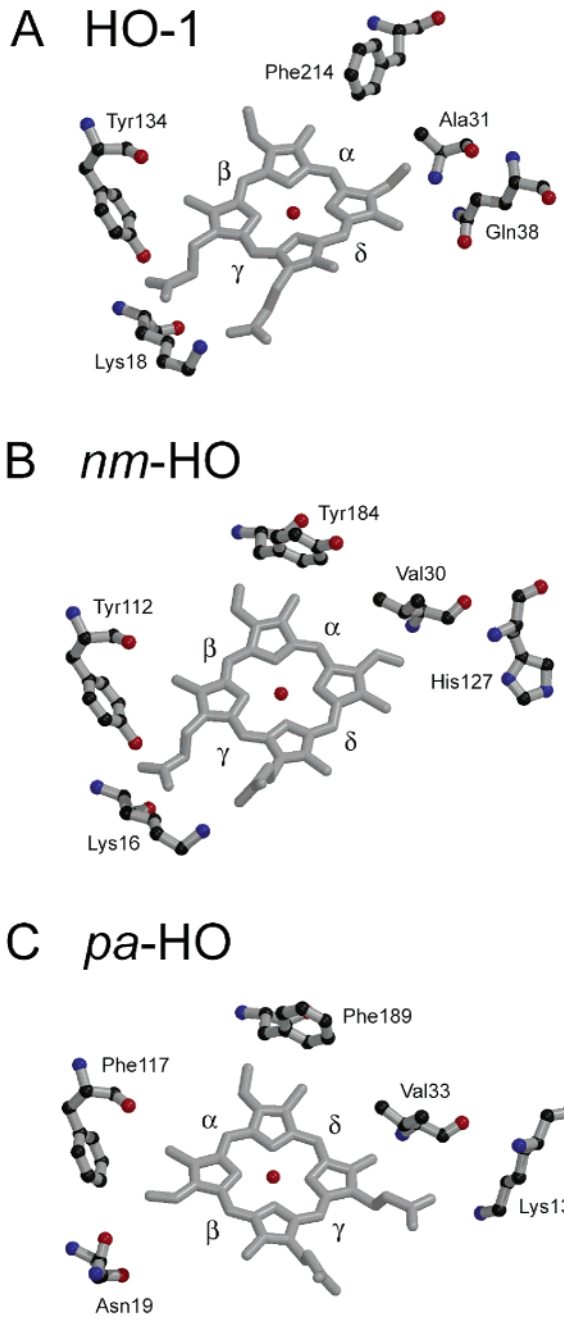

FIGURE 6: Diagram indicating the relative orientations of heme and the heme propionate interactions in **(**A**)** human HO-1, **(**B**)** *nm*-HO, and **(**C**)** *pa*-HO.

Table 2: Heme−Protein Interactions at a Distance of 4.0 Å or Less in Various Heme Oxygenases[a]

heme position	HO-1	*nm*-HO	*pa*-HO
1-methyl	Gln38	Phe123	Phe189
2-vinyl	Met34	Val30	Phe189
3-methyl	Phe214	Tyr184	Phe117
4-vinyl	Thr135	Tyr184	Phe117
5-methyl	Tyr134	Phe181	Leu124
6-propionate	Arg183	Tyr112	solvent
7-propionate	Lys18	Lys16	Lys132
8-methyl	Val146	None	Val33

[a] See Figure 1 for heme numbering. Residues in boldface type represent conserved interactions shared by all three Hos.

contacts may provide some additional stability to the heme orientation. The minor β-biliverdin product arises from 180°

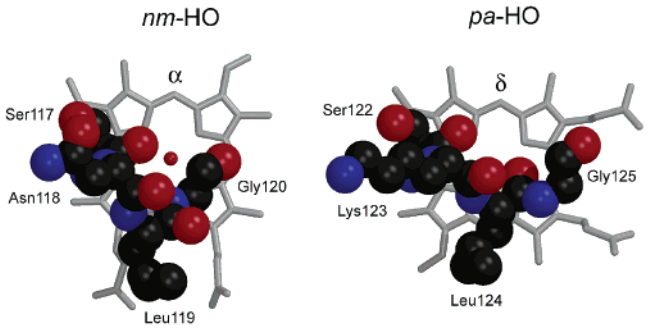

FIGURE 7: CPK model showing distal helix residues above the heme surface in *nm*-HO (left) and *pa*-HO (right), which block access to all but one *meso* carbon.

rotation of the heme substrate about the α−γ *meso* axis (*28*), as previously observed in human HO-1 (*44*) and more recently in the crystal structure of bacterial *cd*-HO (*7*).

CONCLUSIONS

Given the close structural homology between the various HOs whose structures are known, it is reasonable to expect a common mechanism for the control of regioselecitivity. Three obvious factors related to regioselective hydroxylation are shared by all HOs. First, the distal helix blocks reaction with the iron-linked hydroperoxy intermediate at all but the *meso* heme carbon to be hydroxylated (Figure 7). Second, the distal helix favors bending of the Fe(III)-OOH intermediate toward the correct *meso* carbon. Third, the local solvent−protein hydrogen-bonded network also favors bending of the Fe(III)-OOH toward the correct *meso* carbon in addition to providing the proton relay network required for oxygen activation.

The main new insight in this study is that only minor alterations on the surface of HO can lead to different regioselective hydroxylation of the heme substrate. The *nm*-HO and *pa*-HO structures are very similar, yet *nm*-HO gives the more common α-meso hydroxylated product while *pa*-HO hydroxylates primarily the *δ-meso* carbon. This difference is due to a rotation of the heme within a common active-site pocket. The heme orientation is controlled by the positioning of surface Lys and Arg residues that interact with the heme propionates. These interactions are very likely not strong since they occur on the surface where bulk solvent can provide a dielectric screen. A relatively loose association is actually an advantage since this ensures an energetically easier release of product under turnover conditions.

ACKNOWLEDGMENT

We thank Dr. Alexander McPherson for specific advice in the crystallization of *pa*-HO and Dr. Maolin Guo and Weiping Yang for helpful discussions and technical assistance.

REFERENCES

1. Davydov, R. M., Yoshida, T., Ikeda-Saito, M., and Hoffman, B. M. (1999) Hydroperoxy-heme oxygenase generated by cryoreduction catalyzes the formation of α-*meso*-hydroxyheme as detected by EPR and ENDOR, *J. Am. Chem. Soc. 121*, 10656−10657.
2. Ortiz de Montellano, P. R. (1998) Heme oxygenase mechanism: evidence for an electrophilic ferric peroxide species, *Acc. Chem. Res. 31*, 543−549.
3. Sono, M., Roach, M. P., Coulter, E. D., and Dawson, J. H. (1996) Heme-containing Oxygenases, *Chem. Rev. 96*, 2841−2888.

4. Schuller, D. J., Wilks, A., Ortiz de Montellano, P. R., and Poulos, T. L. (1999) Crystal structure of human heme oxygenase-1, *Nat. Struct. Biol. 6*, 860−867.
5. Sugishima, M., Omata, Y., Kakuta, Y., Sakamoto, H., Noguchi, M., and Fukuyama, K. (2000) Crystal structure of rat heme oxygenase-1 in complex with heme, *FEBS Lett. 471*, 61−66.
6. Schuller, D. J., Zhu, W., Stojiljkovic, I., Wilks, A., and Poulos, T. L. (2001) Crystal Structure of Heme Oxygenase from the Gram-Negative Pathogen *Neisseria meningitidis* and a Comparison with Mammalian Heme Oxygenase-1, *Biochemistry 40*, 11552−11558.
7. Hirotsu, S., Chu, G. C., Unno, M., Lee, D. S., Yoshida, T., Park, S.-Y., Shiro, Y., and Ikeda-Saito, M. (2003) The crystal structures of the ferric and ferrous forms of the heme complex of HmuO, a heme oxygenase of *Corynebacterium diphtheriae*, *J. Biol. Chem.* (in press).
8. Matera, K. M., Takahashi, S., Fujii, H., Zhou, H., Ishikawa, K., Yoshimura, T., Rousseau, D. L., Yoshida, T., and Ikeda-Saito, M. (1996) Oxygen and one reducing equivalent are both required for the conversion of alpha-hydroxyhemin to verdoheme in heme oxygenase, *J. Biol. Chem. 271*, 6618−6624.
9. Liu, Y., Moënne-Loccoz, P., Loehr, T. M., and Ortiz de Montellano, P. R. (1997) Heme oxygenase-1, intermediates in verdoheme formation and the requirement for reduction equivalents, *J. Biol. Chem. 272*, 6909−6917.
10. Liu, Y., and Ortiz de Montellano, P. R. (2000) Reaction intermediates and single turnover rate constants for the oxidation of heme by human heme oxygenase-1, *J. Biol. Chem. 275*, 5297−5307.
11. Ortiz de Montellano, P. R. (2000) The mechanism of heme oxygenase, *Curr. Opin. Chem. Biol. 4*, 221−227.
12. Ortiz de Montellano, P. R., and Wilks, A. (2001) in *Advances in Inorganic Chemistry*, pp 359−407, Academic Press Inc, San Diego, CA.
13. Cornejo, J., Willows, R. D., and Beale, S. I. (1998) Phytobilin biosynthesis: cloning and expression of a gene encoding soluble ferredoxin-dependent heme oxygenase from *Synechocystis* sp. PCC 6803, *Plant J. 15*, 99−107.
14. Friebe, A., Schultz, G., and Koesling, D. (1996) Sensitizing soluble guanylyl cyclase to become a highly CO-sensitive enzyme, *EMBO J. 15*, 6863−6868.
15. Ingi, T., and Ronett, G. V. (1995) Direct demonstration of a physiological role for carbon monoxide in olfactory receptor neurons, *J. Neurosci. 15*, 8214−8222.
16. Ryter, S. W., Otterbein, L. E., Morse, D., and Choi, A. M. K. (2002) Heme oxygenase/carbon monoxide signaling pathways: Regulation and functional significance, *Mol. Cell. Biochem. 234*, 249−263.
17. Verma, A., Hirsch, D. J., Glatt, C. E., Ronnett, G. V., and Snyder, S. H. (1993) Carbon monoxide: a putative neural messenger, *Science 259*, 381−384.
18. Zakhary, R., Poss, K. D., Jaffrey, S. R., Ferris, C. D., Tonegawa, S., and Snyder, S. H. (1997) Targeted gene deletion of heme oxygenase 2 reveals neural role for carbon monoxide, *Proc. Natl. Acad. Sci. U.S.A. 94*, 14848−14853.
19. Dore, S., Takahashi, M., Ferris, C. D., Hester, L. D., Guastella, D., and Snyder, S. H. (1999) Bilirubin, formed by activation of heme oxygenase-2, protects neurons against oxidative stress injury, *Proc. Natl. Acad. Sci. U.S.A. 96*, 2445−2450.
20. Stocker, R., Yamamoto, Y., McDonagh, A. F., Glazer, A. N., and Ames, B. N. (1987) Bilirubin is an antioxidant of possible physiological importance, *Science 235*, 1043−1046.
21. Yachie, A., Niida, Y., Wada, T., Igarashi, N., Kaneda, H., Toma, T., Ohta, K., Kasahara, Y., and Koizumi, S. (1999) Oxidative stress causes enhanced endothelial cell injury in human heme oxygenase-1 deficiency, *J. Clin. Invest. 103*, 129−135.
22. Zhu, W., Hunt, D. J., Richardson, A. R., and Stojiljkovic, I. (2000) Use of heme compounds as iron sources by pathogenic *Neisseriae* requires the product of the *hemO* gene, *J. Bacteriol. 182*, 439−447.
23. Ratliff, M., Zhu, W. M., Deshmukh, R., Wilks, A., and Stojiljkovic, I. (2001) Homologues of *neisserial* heme oxygenase in gram-negative bacteria: Degradation of heme by the product of the pigA gene of *Pseudomonas aeruginosa*, *J. Bacteriol. 183*, 6394−6403.
24. Davies, J. C. (2002) *Pseudomonas aeruginosa* in cystic fibrosis: pathogenesis and persistance, *Paediatr. Respir. Rev. 3*, 128−134.
25. Ochsner, U. A., Johnson, Z., and Vasil, M. L. (2000) Genetics and Regulation of Two Distinct Haem-Uptake Systems, Phu and Has, in *Pseudomonas aeruginosa*, *Microbiology 146*, 185−198.
26. Vasil, M. L., and Ochsner, U. A. (1999) The response of *Pseudomonas aeruginosa* to iron: genetics, biochemistry, and virulence, *Mol. Microbiol. 34*, 399−413.
27. Farnaud, S., and Evans, R. W. (2003) Lactoferrin—a multifunctional protein with antimicrobial properties, *Mol. Immunol. 40*, 395−405.
28. Caignan, G. A., Deshmukh, R., Wilks, A., Zeng, Y., Huang, H. W., Moenne-Loccoz, P., Bunce, R. A., Eastman, M. A., and Rivera, M. (2002) Oxidation of Heme to beta- and delta-Biliverdin by *Pseudomonas aeruginosa* Heme Oxygenase as a Consequence of an Unusual Seating of the Heme, *J. Am. Chem. Soc. 124*, 14879−14892.
29. Wilks, A., Black, S. M., Miller, W. L., and Ortiz de Montellano, P. R. (1995) Expression and characterization of truncated human heme oxygenase hHO-1 and a fusion protein of hHO-1 with human cytochrome P450 reductase, *Biochemistry 34*, 4421−4427.
30. Wilks, A., and Schmitt, M. P. (1998) Expression and characterization of a heme oxygenase (Hmu O) from *Corynebacterium diphtheriae*, *J. Biol. Chem. 273*, 837−841.
31. Zhu, W., Wilks, A., and Stojiljkovic, I. (2000) Degradation of heme in gram-negative bacteria: the product of the hemO gene of *Neisseriae* is a heme oxygenase, *J. Bacteriol. 182*, 6783−6790.
32. Zhou, H., Migita, C. T., Sato, M., Sun, D., Zhang, X., Ikeda-Saito, M., Fujii, H., and Yoshida, T. (2000) Participation of carboxylate amino acid side chain in regiospecific oxidation of heme by heme oxygenase, *J. Am. Chem. Soc. 122*, 8311−8312.
33. Otwinowski, Z., and Minor, W. (1997) Processing of X-ray diffraction data collected in oscillation mode, *Methods Enzymol. 276*, 307−326.
34. Collaborative Computational Project, N. (1994) *Acta Crystallogr. D50*, 760−767.
35. de La Fortelle, E., and Bricogne, G. (1997) SHARP, *Methods Enzymol. 276*, 472−494.
36. Jones, T. A., Zou, J. Y., Cowan, S. W., and Kjeldgaard, M. (1991) Improved methods for building protein models in electron density maps and the location of errors in these models, *Acta Crystallogr. A47*, 110−119.
37. Brunger, A. T., Adams, P. D., Clore, G. M., DeLano, W. L., Gros, P., Grosse-Kunstleve, R. W., Jiang, J.-S., Kuszewski, R. F., Nilges, M., Pannu, N. S., Read, R. J., Rice, R. J., Rice, L. M., Simonson, T., and Warren, G. L. (1998) Crystallography & NMR System: A new software suite for macromolecular structure determination, *Acta Crystallogr. D54*, 905−921.
38. Laskowski, R. A., MacArthur, M. W., and Thornton, J. M. (1998) Validation of protein models derived from experiment, *Curr. Opin. Struct. Biol. 8*, 631−639.
39. Wilks, A. (2002) Heme oxygenase: evolution, structure, and mechanism, *Antioxid. Redox Signal. 4*, 603−614.
40. Colas, C., and Ortiz de Montellano, P. R. (2003) Autocatalytic radical reactions in physiological prosthetic heme modification, *Chem. Rev. 103*, 2305−2332.
41. Lad, L., Schuller, D. J., Shimizu, H., Friedman, J., Li, H., Ortiz de Montellano, P. R., and Poulos, T. L. (2003) Comparison of the heme-free and -bound crystal structures of human heme oxygenase-1, *J. Biol. Chem. 278*, 7834−7843.
42. Sugishima, M., Sakamoto, H., Kakuta, Y., Omata, Y., Hayashi, S., Noguchi, M., and Fukuyama, K. (2002) Crystal structure of rat apo-heme oxygenase-1 (HO-1): Mechanism of heme binding in HO-1 inferred from structural comparison of the apo and heme complex forms, *Biochemistry 41*, 7293−7300.
43. Friedman, J., Lad, L., Deshmukh, R., Li, H., Wilks, A., and Poulos, T. L. (2003) Crystal structures of the NO- and CO-bound heme oxygenase from *Neisseriae meningitidis*: Implications for O_2 activation, *J. Biol. Chem. 278*, 34654−34659.
44. Hernandez, G., Wilks, A., Paolesse, R., Smith, K. M., Ortiz de Montellano, P. R., and La Mar, G. N. (1994) Proton NMR investigation of substrate-bound heme oxygenase: evidence for electronic and steric contributions to stereoselective heme cleavage, *Biochemistry 33*, 6631−6641.
45. Fujii, H., Zhang, X., and Yoshida, T. (2004) Essential Amino Acid Residues Controlling the Unique Regioselectivity of Heme Oxygenase in *Pseudomonas aeruginosa*, *J. Am. Chem. Soc.* (in press).
46. Esnouf, R. M. (1997) An extensively modified version of MolScript that includes greatly enhanced coloring capabilities, *J. Mol. Graph. Model. 15*, 132−134.
47. Esnouf, R. M. (1999) Further additions to MolScript version 1.4, including reading and contouring of electron-density maps, *Acta Crystallogr. D55*, 938−940.

BI049687G